Supporting Information

Title: Targeted Delivery of Gemcitabine to Lung Cancer Cells via a Hyaluronic Acid-Based Nanoplatform

Author: Fengbo Yu [a,b], Jingdan Cao [b], Xingjun Fan [d], Junxia Gao [c], Guifang Liu [b], Chonghuan Lin [b], Ying Zhu [b], Qiang Wang [c*]

Author affiliations: [a] Collaborative Innovation Center for Development and Application of Northern Medicine Resources, Mudanjiang Medical University, Mudanjiang, Heilongjiang Province, People's Republic of China; [b] School of Pharmacy, Mudanjiang Medical University, Mudanjiang, Heilongjiang Province, People's Republic of China; [c] Hongqi Hospital, Mudanjiang Medical University, Mudanjiang, Heilongjiang Province, People's Republic of China. [d] School of Public Health, Mudanjiang Medical University, Mudanjiang, Heilongjiang Province, People's Republic of China.

Correspondence: Qiang Wang

[c] Hongqi Hospital, Mudanjiang Medical University, Mudanjiang, Heilongjiang Province, People's Republic of China.

Email: drwang1982@126.com

File List:

1. UV-Vis Scanning Spectra and Standard Curve of Gemcitabine (GEM)

2. HPLC Chromatograms of HA-PSI at Different Reaction Time Points

3. FT-IR and SEM Characterization of HAP

4. SEM Analysis of HA-PSI/HAP Ratios in Self-Assembled Nanoparticles

5. Results of Single-Factor Optimization Experiments

6. Concentration Optimization of GEM@(HAP/PSI) and GEM@HA-(HAP/PSI) Formulations

1. UV-Vis Scanning Spectra and Standard Curve of Gemcitabine (GEM)

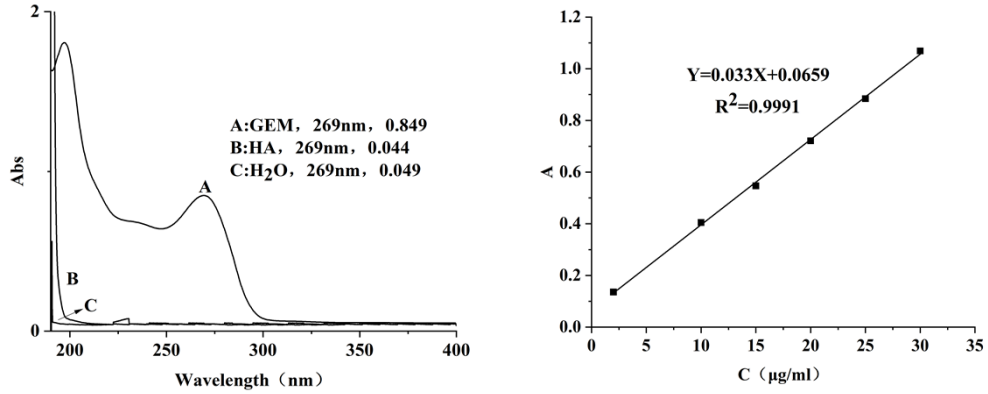

Figure S1 Ultraviolet scanning spectra and standard curve of Gemcitabine (GEM)

As Figure S1 shows, 269 nm was selected as the detection wavelength for GEM. The standard curve of GEM was A=0.033 C+0.0659, with R^2=0.9991. The linearity was good in the concentration range of 2–30 μg/mL.

2. HPLC Chromatograms of HA-PSI at Different Reaction Time Points

The reaction endpoint was determined through HPLC-ELSD analysis following protocol validation with blank and standard samples. Optimized chromatographic conditions for HA quantification were implemented as follows: carrier gas, hydrogen (1.5 L/min flow rate); drift tube temperature, 60℃; mobile phase, acetonitrile/water (85:15, v/v) at 0.6 mL/min; column, C18 reversed-phase column (Kromasil 100-5C18, 250 × 4.6 mm, E91750); and injection parameters, 20 μL of a 0.2 mg/mL sample solution. Systematic sampling was performed by collecting reaction supernatants at predetermined intervals (0, 6, 12 and 18 h). Subsequent chromatographic analysis enabled the simultaneous quantification of residual HA in the supernatant phase. Reaction completion was confirmed when HA consumption reached equilibrium, as evidenced by stabilized chromatographic peak area ratios between consecutive time points.

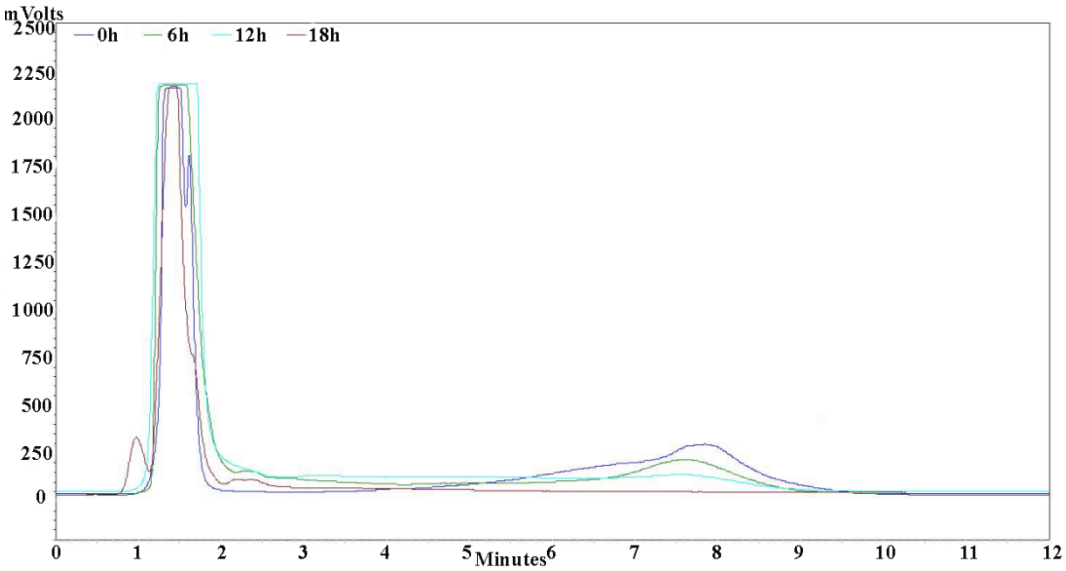

Figure S2 Monitoring of HA content changes

Figure S2 shows the chromatograms at different time points during the synthesis of HA-PSI_{10}. As shown in the figure, the solvent peak appeared at 1 min and the HA peak around 6 min 40 S. After 18 h, the HA peak disappeared completely, indicating that the HA molecules were fully incorporated into the PSI molecules. Therefore, the reaction termination time for HA and PSI was set to 18 h. Given that the amount of HA incorporated into the structures of HA-PSI_{20} and HA-PSI_{40} was less than that of HA-PSI_{10}, this reaction time was also set to 18 hours.

3. FT-IR and SEM Characterization of HAP

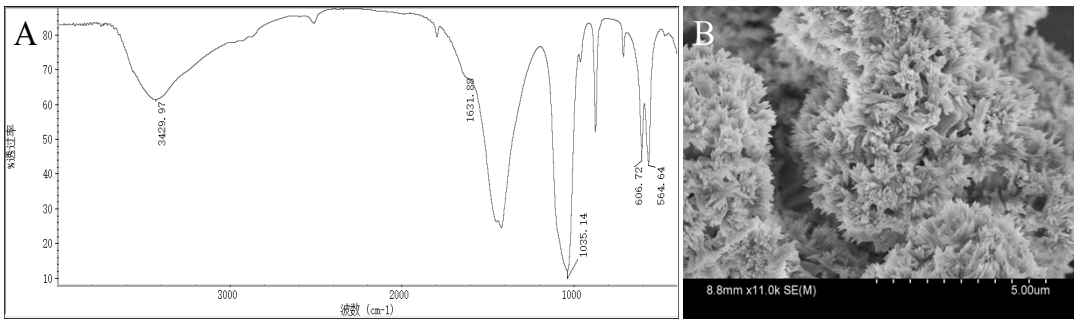

Figure S3 Characterization spectras of HAP (A: FTIR; B: SEM)

Figure S3 presents the Fourier-transform infrared (FT-IR) spectrum and scanning electron microscopy (SEM) image of the synthesized hydroxyapatite (HAP). The FT-IR spectrum (Figure S3A) confirms the successful formation of HAP, showing characteristic peaks consistent with our previous findings. Broad bands observed at 3429 cm^{-1} and 1631 cm^{-1} are attributed to the stretching and bending vibrations of adsorbed water (O–H),

respectively. The strong, prominent peak at 1035 cm^{-1} corresponds to the asymmetric stretching vibration (ν_3) of the phosphate (PO_4^{3-}) group. Furthermore, the distinct doublet at 606 cm^{-1} and 564 cm^{-1} is assigned to the bending vibration (ν_4) of the O–P–O bonds within the phosphate tetrahedron. This set of spectral features is characteristic of crystalline hydroxyapatite. The corresponding SEM image (Figure S3B) reveals the morphology of the synthesized product, showing that the HAP particles exist in an agglomerated state.

4. SEM Analysis of HA-PSI/HAP Ratios in Self-Assembled Nanoparticles

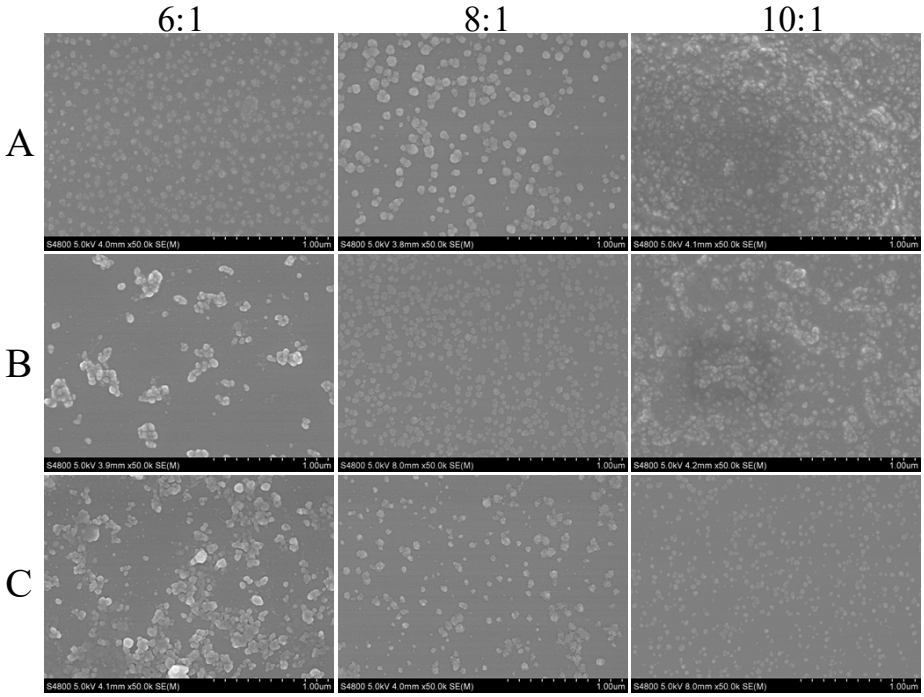

Figure S4 SEM results of HA-PSI:HAP at different ratios (A: HA-$(HAP/PSI)_{40}$; B: HA-$(HAP/PSI)_{20}$; C: HA-$(HAP/PSI)_{10}$)

Based on previous studies of (HAP/PSI) and functionalized X-(HAP/PSI) complexes, HA-(HAP/PSI) nanoparticles were prepared using three different mass ratios of HA-PSI to HAP: 6:1, 8:1, and 10:1, followed by morphological characterization via SEM. As shown in Figure S4, all formulations successfully self-assembled into relatively uniform nanostructures. Specifically, HA-PSI_{40} at a 6:1 ratio, HA-PSI_{20} at an 8:1 ratio, and HA-PSI_{10} at a 10:1 ratio each formed nanoparticles with consistent morphology.

5. Results of Single-Factor Optimization Experiments

Table S1 Effect of GEM concentration on drug loading (n=3)

C_{GEM}（mg/mL）	EE%	DLC%
5	18.29±1.73	15.49±1.39

C_{GEM}（mg/mL）	EE%	DLC%
10	24.01±0.92	32.29±0.82
20	26.28±1.65	51.05±1.57
30	27.47±2.17	61.96±1.96
40	32.92±2.47	72.45±1.43
50	19.30±1.79	65.83±2.06

Abbreviations: C, concentration; GEM, gemcitabine; EE, encapsulation efficiency; DLC, drug loading capacity.

As shown in Table S1, when the HAP concentration was fixed, the drug loading capacity reached its maximum at a drug concentration of 40 mg/mL. In contrast, the encapsulation efficiency initially decreased, then increased to a higher value at 40 mg/mL, before declining again at 50 mg/mL.

Table S2 Effects of HAP concentrations on encapsulation rate and drug loading（n=3）

C_{HAP}（mg/mL）	EE%	DLC%
1	8.24±1.15	76.12±1.93
2	12.26±1.37	70.63±2.48
3	28.92±1.89	79.25±1.00
5	32.92±2.47	72.45±1.43
8	16.82±1.53	45.60±2.41
10	12.66±1.05	33.57±1.88
15	11.09±1.18	22.78±1.90

Abbreviations: C, concentration; HAP, hydroxyapatite; EE, encapsulation efficiency; DLC, drug loading capacity.

According to the data presented in Table S2, with a fixed concentration of gemcitabine hydrochloride, the encapsulation efficiency of the formulation improved as the HAP concentration increased, reaching a maximum when the HAP concentration attained 5 mg/mL. In contrast, the drug loading capacity exhibited a gradual decline with increasing HAP concentration.

Table S3 Effect of adsorption time on encapsulation rate and drug loading (n=3)

Time（min）	EE%	DLC%
10	32.92±2.47	72.45±1.43
20	30.76±1.18	70.95±0.83
40	29.57±0.74	70.18±0.48
60	31.21±1.13	71.38±0.75

Abbreviations: EE, encapsulation efficiency; DLC, drug loading capacity.

Based on the results in Table S3, when both the drug and HAP concentrations were fixed, the drug loading capacity and encapsulation efficiency reached a relative equilibrium and saturation at the 10-minute time point.

6. Concentration Optimization of GEM@(HAP/PSI) and GEM@HA-(HAP/PSI) Formulations

Based on the results of the single-factor investigations, the final formulation and manufacturing process for GEM@(HAP/PSI) were optimized using a Box-Behnken Design (BBD). Drug concentration (A, 30-50 mg/mL), HAP concentration (B, 3-8 mg/mL), and the PSI-to-HAP mass ratio (C, 3:1-8:1) were selected as the critical factors for the experimental design. The corresponding response surface plots were generated to determine the optimal parameters. Subsequently, the formulation process for GEM@HA-(HAP/PSI) was optimized using a Central Composite Design (CCD). This design considered drug concentration (A, 30-50 mg/mL) and HAP concentration (B, 3-8 mg/mL) as variables, while maintaining fixed mass ratios between the HA-PSI conjugates and HAP: a 6:1 ratio for HA-PSI_{40}, an 8:1 ratio for HA-PSI_{20}, and a 10:1 ratio for HA-PSI_{10}.

Table S4 p-values and F values for different preparation methods

Source			Model	A	B	C	AB	AC	BC	A^2	B^2	C^2	Lack of Fit
GEM@(HAP/PSI)	**EE**	p-value	< 0.0001	< 0.0001	< 0.0001	< 0.0001	0.1211	0.0005	0.0193	< 0.0001	< 0.0001	0.0002	0.8319
		F value	139.66	202.58	340.24	63.17	3.11	36.77	9.14	206.80	289.91	49.87	0.2893
	DLC	p-value	< 0.0001	0.0027	0.0015	0.0080	0.0678	0.0038	< 0.0001	< 0.0001	< 0.0001	< 0.0001	0.2107
		F value	77.01	20.62	25.11	13.42	4.66	18.12	591.91	277.13	318.98	77.01	2.38
GEM@HA-$(HAP/PSI)_{40}$	**EE**	p-value	< 0.0001	< 0.0001	< 0.0001	-	0.6836	-	-	0.0001	< 0.0001	-	0.4808
		F value	189.18	193.10	156.70	-	0.1806	-	-	56.90	345.67	-	0.9946
	DLC	p-value	< 0.0001	0.0103	< 0.0001	-	0.0078	-	-	< 0.0001	< 0.0001	-	0.3137
		F value	179.87	12.08	66.29	-	13.56	-	-	237.12	262.90	-	1.65
GEM@HA-$(HAP/PSI)_{20}$	**EE**	p-value	< 0.0001	0.0003	0.0002	-	0.0036	-	-	< 0.0001	< 0.0001	-	0.4144
		F value	80.12	43.11	48.07	-	18.36	-	-	80.01	100.49	-	1.21
	DLC	p-value	< 0.0001	0.0025	0.0009	-	0.6044	-	-	< 0.0001	< 0.0001	-	0.2479
		F value	150.25	21.11	29.84	-	0.2941	-	-	305.66	136.91	-	2.06
GEM@HA-$(HAP/PSI)_{10}$	**EE**	p-value	< 0.0001	0.0332	< 0.0001	-	0.2706	-	-	< 0.0001	0.0002	-	0.7896
		F value	180.13	6.99	121.34	-	1.43	-	-	490.04	49.86	-	0.3546
	DLC	p-value	< 0.0001	0.0016	0.4709	-	0.0620	-	-	< 0.0001	0.0002	-	0.3660
		F value	88.21	24.87	0.5809	-	4.92	-	-	222.85	48.78	-	1.40

Abbreviations: GEM, gemcitabine; HA, hyaluronic acid; HAP, hydroxyapatite; PSI, polysuccinimide; EE, encapsulation efficiency; DLC, drug loading capacity. **Note:** P-values > 0.05 are not significant, P-values < 0.05 are significant, and P-values < 0.001 are extremely significant.

As shown in Table S4, the "Model" terms for all materials exhibited p-values < 0.0001 and high F-values (ranging from 77.01 to 189.18) for both EE and DLC. This indicates that the established response surface models are highly significant and can effectively describe the relationships between the factors (A, B, C, etc.) and the response values. The "Lack of Fit" terms for all models showed p-values > 0.1 (0.2107-0.8319) and low F-values, confirming that the lack of fit is not significant. This demonstrates good model fit, minimal unexplained variation, and high reliability and predictive capability of the models.

For GEM@(HAP/PSI), factors A, B, and C all exhibited highly significant main effects ($p < 0.01$) on both EE and DLC, indicating that all three investigated factors are key variables influencing encapsulation and drug loading. By comparing the F-values, HAP concentration (B) was identified as the most critical single factor affecting EE, followed by drug concentration (A). The AC and BC interactions were significant ($p < 0.05$) for both EE and DLC, suggesting synergistic or antagonistic effects between these factors.

For the GEM@HA-(HAP/PSI) series, factors A and B showed highly significant main effects ($p < 0.01$) on both EE and DLC across all formulations, confirming their roles as key variables. All significant quadratic terms (A^2, B^2) had p-values < 0.0001, indicating that the influence of these factors on the responses (EE and DLC) is not linear but follows a strong curved relationship (i.e., the existence of an optimum point). This implies that each factor has an optimal level, with deviations leading to decreased performance. Notable variations were observed among the different HA-modified formulations. For GEM@HA-$(HAP/PSI)_{10}$, factor B had an extremely significant effect on EE ($F = 121.34$) but no significant effect on DLC ($p = 0.4709$), suggesting that HAP concentration has a minimal impact on drug loading in this specific formulation. Furthermore, the significance of factor A for EE decreased from $p < 0.0001$ in GEM@HA-$(HAP/PSI)_{40}$ to $p = 0.0332$ in GEM@HA-$(HAP/PSI)_{10}$. This shift in significance patterns suggests that the relative importance of the factors changes with the amount of HA modification, leading to non-identical optimal process conditions for EE and DLC across the nano-formulation series, necessitating multi-objective optimization or trade-offs. The AB interaction term was significant in the EE model for GEM@HA-$(HAP/PSI)_{20}$ ($p = 0.0036$) and the DLC model for GEM@HA-$(HAP/PSI)_{40}$ ($p = 0.0078$), indicating a clear

synergistic effect between the two factors in these specific formulations. In other cases, the significance of AB was reduced or became non-significant (e.g., p = 0.6836, 0.2706), implying that the interaction between the factors weakened and their effects became more independent.

In summary, across all formulations, drug concentration (A) and HAP concentration (B) were the primary significant factors affecting both EE and DLC ($p < 0.01$ in most cases). The quadratic terms (A^2, B^2) were extremely significant ($p < 0.001$) in all models, confirming the existence of well-defined optimal points (e.g., maxima or minima) on the response surfaces.

Table S5 Model summary statistics

Nano formulations \ Response		R^2	Adj R^2	Pred R^2	Adequate Precision	C.V. %
GEM@(HAP/PSI)	**EE**	0.9945	0.9873	0.9771	33.8708	3.98
	DLC	0.9953	0.9892	0.9491	34.5695	2.86
GEM@HA-$(HAP/PSI)_{10}$	**EE**	0.9927	0.9874	0.9707	40.3779	3.90
	DLC	0.9923	0.9868	0.9654	37.6916	2.74
GEM@HA-$(HAP/PSI)_{20}$	**EE**	0.9828	0.9706	0.9045	21.7600	5.94
	DLC	0.9908	0.9842	0.9543	32.2910	3.58
GEM@HA-$(HAP/PSI)_{40}$	**EE**	0.9923	0.9868	0.9746	35.3149	4.86
	DLC	0.9844	0.9732	0.9218	24.4959	4.69

Abbreviations: GEM, gemcitabine; HA, hyaluronic acid; HAP, hydroxyapatite; PSI, polysuccinimide; EE, encapsulation efficiency; DLC, drug loading capacity. **Note:** P-values > 0.05 are not significant, P-values < 0.05 are significant, and P-values < 0.001 are extremely significant.

The evaluation of model goodness-of-fit (Table S5) demonstrated that all response surface models exhibited R^2 values greater than 0.98, indicating their ability to explain the vast majority of the variation in the response values. The close agreement between the adjusted R^2 and R^2 values confirmed the absence of overfitting. More critically, the predicted R^2 for all models exceeded 0.90, with the majority surpassing 0.95, affirming the models' excellent predictive capability. The exceptionally high adequate precision values (all > 20) signify a sufficient signal-to-noise ratio, making the models reliable for navigating the design space. Furthermore, the low coefficients of variation (C.V.% < 6%) reflect good reproducibility of the experimental data. Collectively, these statistical metrics validate the high reliability of the established quadratic models for subsequent formulation optimization and prediction.